Journal of Statistical Physics, Vol. 59, Nos. 5/6, 1990

Finite-Size Scaling of the Three-State Potts Model on a Simple Cubic Lattice

M. Fukugita,[1] H. Mino,[2] M. Okawa,[2] and A. Ukawa[3]

Received September 26, 1989; revision received January 8, 1990

Finite-size scaling is studied for the three-state Potts model on a simple cubic lattice. We show that the specific heat and the magnetic susceptibility scale accurately as the volume. The correlation length exhibits behaviors expected for a genuine first-order transition; the one extracted from the unsubtracted correlation function shows a characteristic finite-size behavior, whereas the physical correlation length that characterizes the first excited state stays at a finite value and is discontinuous at the transition point.

KEY WORDS: Potts model; finite-size scaling; Monte Carlo simulation.

1. INTRODUCTION

The Potts model[1] (see ref. 2 for a review) has attracted the interest of statistical physicists for many years because it represents the simplest extension of the Ising model. In particular, the three-state ($q=3$) Potts model in three dimensions ($d=3$) is one of the most interesting cases in that it is marginal in several respects. According to the Landau theory,[3] the $q=3$ Potts model is predicted to have a first-order phase transition regardless of the value of d. In $d=2$, however, the model has been proven[4] to have a second-order phase transition. On the other hand, for $d \geqslant 4$, we expect with confidence that the mean field result is valid and the transition is first order. The case of $d=3$ is subtle, just in between these two cases, for which large fluctuations may still occur in the vicinity of the transition point, while a first-order transition is typically characterized by the absence of critical fluctuations.

The order of the transition of the $d=3$ three-state Potts model has

[1] Research Institute for Fundamental Physics, Kyoto University, Kyoto 606, Japan.
[2] National Laboratory for High Energy Physics (KEK), Ibaraki 305, Japan.
[3] Institute of Physics, University of Tsukuba, Ibaraki 305, Japan.

0022-4715/90/0600-1397$06.00/0

been studied by a variety of methods[2] and a general consensus has been reached that it possesses a weak first-order transition. This mainly came from Monte Carlo studies[5–8] of the system, which found a small but clear jump of the internal energy and the order parameter at the transition point. The finite-size behavior of observables from one such study[7] was puzzling, however, as their behavior indicated a correlation length exponent $\nu = 0.4$–0.5 and the observables showed a growth consistent with a power-law divergence; furthermore, it was reported that critical indices of various thermodynamic quantities are subject to hyperscaling with the above correlation length exponent ν. These are the features generally expected for a second-order transition, and some series analyses[9] indeed favored this alternative. The authors of ref. 5 also found evidence for a second-order fixed point in the metastable region in their renormalization group analysis. Several recent numerical studies,[10,11] however, have concluded that the correlation length is finite at the transition point, though it is quite large ($\xi_c \sim 10$). This latter feature may be regarded as reminiscent of large fluctuations in a system close to criticality.

In this paper, we report a high-statistics Monte Carlo study of the $q = 3$ Potts model in three dimensions aimed at a detailed understanding of the nature of its transition. In particular, we examine for this subtle case the finite-size scaling behavior, which is generally well understood both for second-order[12,13] and first-order[14–19] phase transitions. A general obstacle for such a finite-size scaling analysis is that one needs a fine mesh of temperature and high statistics to trace out the temperature dependence of observables, which become progressively singular with an increasing system size. We have circumvented these problems with a recently developed high-speed vector computer and with a use of a technique utilizing the histogram of the spectral density of the states. This method was proposed by McDonald and Singer,[20] and its advantages were emphasized more recently by Ferrenberg and Swendsen.[21] We used lattices of size varying from $L = 16^3$ to 64^3 with typically one to ten million sweeps at each temperature. In addition to the bulk quantities such as the order parameter and susceptibility commonly studied in finite-size scaling analyses, we investigated the behavior of the correlation length. It exhibits quite distinctive finite-size behaviors depending upon whether the phase transition is first or second order. We also examine the question of whether the correlation length for a first-order phase transition diverges or not at the transition point.

As a comparative example we have made a finite-size scaling analysis for the three-dimensional Ising model, which is known to have a typical second-order phase transition. We used lattices of size $L = 16$–48 with moderate statistics.

In Section 2 we describe the formalism and method of simulation. We give a very brief review in Section 3 of the finite-size scaling of thermodynamic quantities to clarify the goal of our analysis, and the results are presented in Section 4. The finite-size behavior of the correlation length is discussed in Section 5. Section 6 is devoted to our conclusions.

2. FORMULATION AND SIMULATION

The Potts model is given by the Hamiltonian

$$H = -\frac{3}{2} \sum_{\langle i,j \rangle} (\delta_{\sigma_i \sigma_j} - 1) \tag{1}$$

where $\langle i, j \rangle$ is the sum over the nearest neighbor spin pairs and the spin variable σ_i takes $q = 3$ states. The statistical system is defined by

$$Z = \exp(-\beta H) \tag{2}$$

with β the inverse temperature $1/T$. The Hamiltonian (1) is also written as

$$H = -\sum_{\langle i,j \rangle} [\mathrm{Re}(s_i s_j^*) - 1] \tag{3}$$

with a Z_3-valued spin variable s_i.

We work on a simple cubic lattice of size $L^3 = V$ with periodic boundary condition imposed for all directions. For updating the configuration we use the heat-bath algorithm, with a speed of 24 million spin updates per second on an HITAC S820/80.

We measure the internal energy per link

$$E = \langle H \rangle / 3V \tag{4}$$

and the specific heat

$$C = \frac{\partial E}{\partial T} = \frac{1}{3VT^2} (\langle H^2 \rangle - \langle H \rangle^2) \tag{5}$$

We consider two definitions of the order parameter. The first is the conventional one used in ref. 6,

$$\Phi_1 = \overline{\mathrm{Re}} \left(\frac{1}{V} \sum_i s_i \right) \tag{6}$$

where $\overline{\mathrm{Re}}$ stands for the projection onto the nearest $Z(3)$ axis on the complex plane; given a complex number z, $\overline{\mathrm{Re}}\, z$ is equal to $\mathrm{Re}\, z$,

$\mathrm{Re}[\exp(-i2\pi/3)z]$, or $\mathrm{Re}[\exp(i2\pi/3)z]$, depending upon whether the phase of z falls within the interval $(-\pi/3, \pi/3)$, $(\pi/3, \pi)$, or $(-\pi, -\pi/3)$. We also use the definition of the order parameter

$$\Phi_2 = \mathrm{Re}\left(\frac{1}{V}\sum_i s_i\right)^3 \tag{7}$$

with Re the normal real part. The latter order parameter appears more natural, in that no artificial procedure is involved in the definition. We discuss the merits and demerits of these two definitions in Section 4. The susceptibilities are defined by

$$\chi_1 = V(\langle \Phi_1^2 \rangle - \langle \Phi_1 \rangle^2) \tag{8}$$

and

$$\chi_2 = V(\langle \Phi_2^2 \rangle - \langle \Phi_2 \rangle^2) \tag{9}$$

We also measure the unsubtracted zero-momentum projected correlation function

$$C(z) = \langle O(z) O(0)^* \rangle \tag{10}$$

with

$$O(z) = L^{-2} \sum_{i \in (x, y) \text{ plane at } z} s_i \tag{11}$$

the average of L^2 spins on a transverse plane located at z. In actually evaluating (10), we use the cubic symmetry and take an average over three directions to increase statistics.

For the Ising model we take the standard normalization

$$H = -\sum_{\langle i, j \rangle} (s_i s_j - 1) \tag{12}$$

with $s_i = \pm 1$, and the system is defined by (2).

In order to calculate physical observables in the vicinity of the transition point for continuous values of the temperature, we have extensively used the histogram method for the spectral density of states.[20,21] This method is based on the identity

$$P(\beta, H) = P(\beta_0, H) \exp[-(\beta - \beta_0) H] \tag{13}$$

valid for the distribution of the energy

$$P(\beta_0, H) = N(H) \exp(-\beta_0 H) \tag{14}$$

with H the Hamiltonian and $N(H)$ the number of configurations with a given value of H, and a simple realization that a Monte Carlo simulation at a certain $\beta = \beta_0$ gives an estimate of the distribution $P(\beta_0, H)$. Once a good estimate of P is obtained from a long Monte Carlo run, the average of the action at nearby β can be calculated with the modified weight (13).

It is straightforward to extend this spectral density method for evaluating not only the action itself, but also a set of other physical valuables $O_1,..., O_n$; one defines the weight in a multiparameter space which refers to $O_1,..., O_n$, i.e., by replacing $P(\beta, H)$ and $N(H)$ with $P(\beta, H, O_1,..., O_n)$ and $N(H, O_1,..., O_n)$ in (13)–(14).

For random numbers we used the M-series[22] based on the primitive polynomial $x^{250} + x^{103} + 1$ with a period of $2^{250} - 1$. The error analysis was made with the jackknife method.[23] In particular, the error propagation in the spectral density method was estimated by applying it to the distribution of P dividing the run into subsamples.

3. FINITE-SIZE SCALING

Conventional arguments[12,13] for finite-size scaling for a second-order transition start with the assumption that the singular part of the free energy depends only on the lattice size L and the correlation length ξ. It then follows that the peak height of the specific heat and the susceptibility scale as

$$C(T_c(L), L) \sim L^{\alpha/\nu} \tag{15}$$

$$\chi(T_c(L), L) \sim L^{\gamma/\nu} \tag{16}$$

with $T_c(L)$ the "pseudo-critical point," e.g., the peak position of C or χ. For the width of the peak $\Gamma(L)$ and the shift of the critical coupling $T_c(L) - T_c(\infty)$ we expect

$$\Gamma(L) \sim L^{-1/\nu} \tag{17}$$

$$T_c(L) - T_c(\infty) \sim L^{-1/\nu} \tag{18}$$

for both C and χ.

At a first-order transition, on the other hand, the physical correlation length ξ is expected to remain finite. Once L exceeds ξ, thermodynamic quantities at $T_c(L)$ are expected[14–19] to depend only on the volume $V = L^d$,

$$C(T_c(L), L) \sim L^d \tag{19}$$

$$\chi(T_c(L), L) \sim L^d \tag{20}$$

$$\Gamma(L) \sim L^{-d} \tag{21}$$

$$T_c(L) - T_c(\infty) \sim L^{-d} \tag{22}$$

This is a natural result if we remember that the singular behavior at a first-order transition is caused by the coexistence of multiple phases, which produces a delta-function singularity in the limit $L \to \infty$. It is interesting to note that the scaling relations (19)–(22) coincide with (15)–(18) if we set $\nu = 1/d$ and $\alpha = \gamma = 1$. Thus, in a finite-size scaling analysis, first- and second-order transitions can be treated in a same manner; the values of exponents differentiate the order of the transition.[4]

In a practical evaluation, we found that the inclusion of a subleading constant term often gives a better fit for first-order transitions. We then fit the data by the form $aV^{\sigma} + c$ for the Potts model. For the Ising model we took only the leading term aV^{σ}, since our statistics is not enough to discuss the subleading terms.

We add a remark here concerning the range of applicability of the spectral density method. It has been argued[21] that the method allows one to cover the entire critical region with a single simulation. From (13) the interval of β accessible is estimated as $|\beta - \beta_0| \leqslant O(\Delta H^{-1})$, with ΔH the width of the energy distribution at the point of simulation β_0. Since $\Delta H \sim (CL^d)^{1/2}$ with C the specific heat, one obtains from (15) and the hyperscaling relation that $|\beta - \beta_0| \leqslant O(L^{-1/\nu})$ for a second-order transition, and $\leqslant O(L^{-d})$ from (19) for a first-order transition. We indeed found that a single simulation of $O(10^6$–$10^7)$ sweeps suffices for the Potts model with the width of the critical region $\delta T_c/T_c \sim 0.001$ at $L = 48$ to cover the whole critical region. We obtained our result from a single run, with other runs used to check its reliability, however. On the other hand, for the Ising model in three dimensions with a second-order transition, which has a much wider critical region of order $\delta T_c/T_c \sim 0.01$ at $L = 48$, a simulation of similar statistics did not yield satisfactory curves of observables beyond $\delta T/T \sim 0.005$ at $L = 48$. Much higher statistics appears to be needed to correctly sample the edges of the energy distribution in this case. To calculate observables at β, we therefore combined two neighboring runs at β_{01} and β_{02} with $\beta_{01} < \beta < \beta_{02}$, assigning a weight

$$\exp\left[-c^2\left(\frac{\beta - \beta_{0i}}{\beta_{01} - \beta_{02}}\right)^2\right], \qquad i = 1, 2$$

with $c = 2$–3 in our Ising model simulations, so that resulting curves smoothly interpolate the data points.

[4] It has been argued[14] that this similarity is caused by the fact that first-order transitions are governed by discontinuity fixed points. The existence of such fixed points has been questioned, however, by several authors[5,24,25] for the temperature-driven first-order phase transition.

4. RESULT

4.1. Basic Characteristics of the Runs

The Monte Carlo runs we made are summarized in Table I. For all the runs except for those on a 64^3 lattice with 1×10^6 sweeps, we see flipflops of the system between the disordered and ordered states. Examples are shown in Fig. 1 for the order parameter $\langle \Phi_1 \rangle$. The distinction between the two states becomes more conspicuous with increasing volume. In particular, the duration of a phase rapidly increases with V. We plot in Fig. 2 the average number of sweeps n_p between a flip and a flop as a function of the volume. This figure shows that it increases exponentially. This is what we expect for a first-order phase transition, because the free energy barrier is proportional to V.

4.2. Internal Energy and Specific Heat

In Figs. 3 and 4 we show the internal energy E and the specific heat divided by the volume C/V as functions of T for various lattice sizes.

Table I. Statistics of Monte Carlo Runs in Units of 10^6 Sweeps

β	$L=16$	$L=22$	$L=24$	$L=26$	$L=30$	$L=36$	$L=42$	$L=48$	$L=64$
Potts model									
0.36685			1						
0.36690			10	1					
0.36695					4	4			
0.36700		1	10		4		4	5	
0.36701								5	1^a
0.367025									$1^a + 1^b + 2$
0.36705									1^b
Ising model									
0.215	1		1			2			
0.218	1		1			2			
0.220	1		1			2		2	
0.22166	1		1			2		2	
0.223	1		1			2		2	
0.224						2		2	
0.225								2	

[a] Disorder start.
[b] Order start.

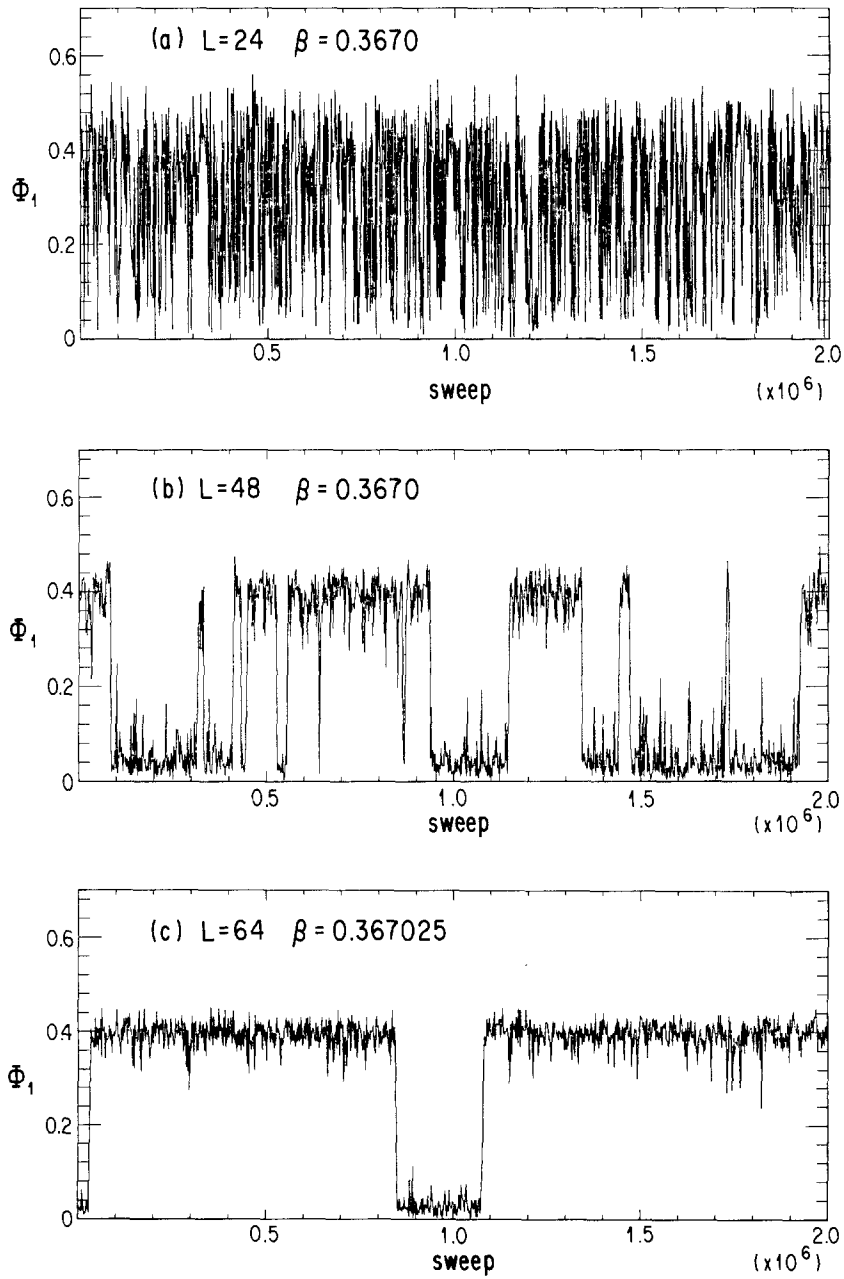

Fig. 1. Time history of the order parameter $\langle \Phi_1 \rangle$. The lattice size and the value of β are listed in figure.

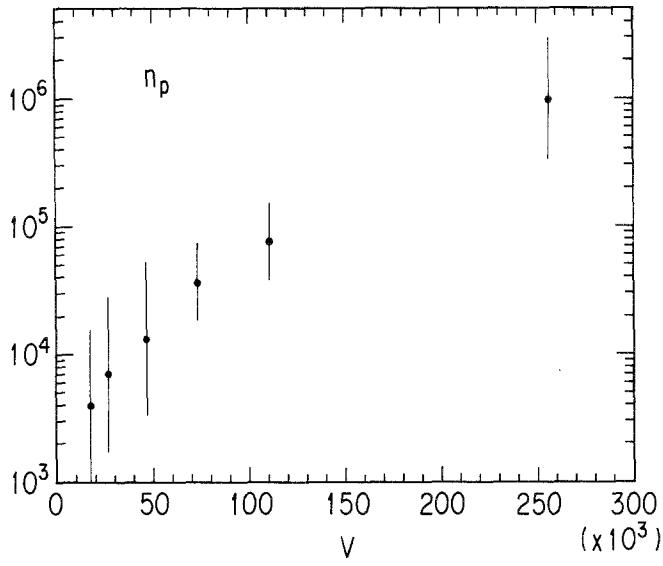

Fig. 2. Average number of sweeps n_p between a flip and a flop as a function of the volume. All the numbers were estimated at $\beta = 0.36700$ except for $L = 26$ ($\beta = 0.36690$) and $L = 36$ ($\beta = 0.36695$).

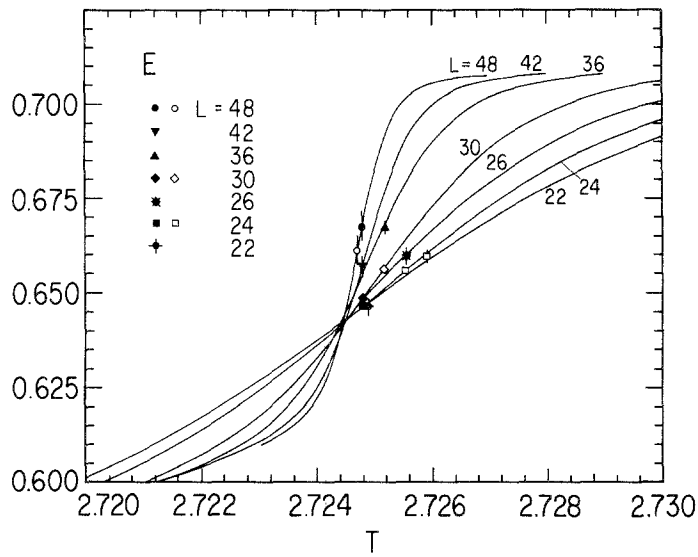

Fig. 3. Internal energy E as a function of T for various lattice sizes. The solid lines show results of the spectral density method using the data represented by the solid symbols as input.

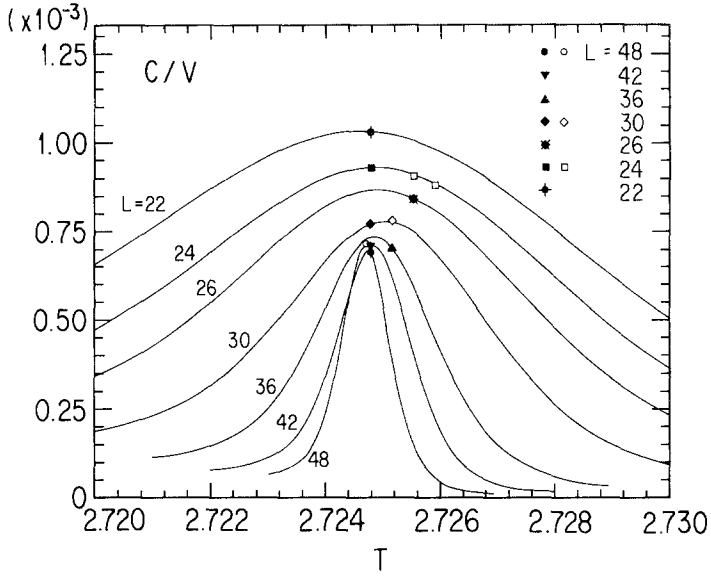

Fig. 4. Specific heat normalized by the volume C/V as a function of T for various lattice sizes. The meaning of the lines and symbols is the same as in Fig. 3.

Figure 3 shows that the variation of the internal energy becomes more abrupt as V increases, indicating that a step-function-type singularity will develop in the infinite-volume limit.

A more quantitative analysis is made in Fig. 4, where we see that the behavior approaches a delta-function-type singularity as V increases. We display in Fig. 5 the height $C_{\max}$ and the inverse of the width $\delta T_{C,1/2}^{-1}$, defined as the full-width at half-maximum, as functions of the volume (see Table II for numerical data). This figure already reveals that $C_{\max}$ and $\delta T_{C,1/2}^{-1}$ scale linearly with the volume very well. We have tested the quality of the linear behavior of $C_{\max}$ and $\delta T_{C,1/2}^{-1}$ by a three-parameter fit of the form $aV^{\sigma}+c$ as well as the two-parameter fit with $\sigma=1$. The result is given in the first two parts of Table III and in Fig. 5, which nicely confirms the linear dependence. In $C_{\max}$ we note an appreciable constant, which is known also in other models.[19,21]

It is interesting to compare this result with that for the three-dimensional Ising model. We present E and C for this case in Figs. 6 and 7, respectively. These figures show a marked contrast with the corresponding ones for the Potts model; in particular, in Fig. 6 we note that the asymptotic curve is approached from below without mutual crossings of curves for different size, in contrast to Fig. 3 for the Potts model. From

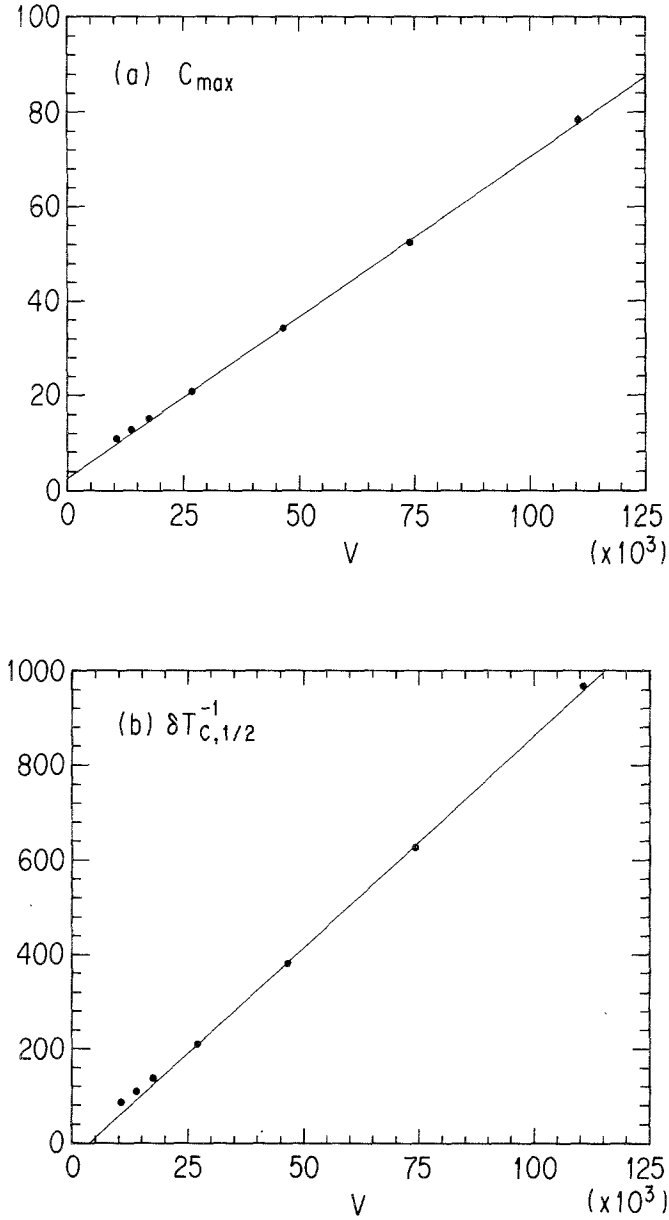

Fig. 5. (a) Peak height of the specific heat C as a function of the volume. The solid line represents the two-parameter fit given in the first part of Table III. (b) Inverse of the peak width of C as a function of the volume. The solid line represents the two-parameter fit given in the second part of Table III.

Table II. Peak Height and Full-Width at Half-Maximum of the Specific Heat, Susceptibilities, and V_L for Potts Model Obtained by the Spectral Density Method

	$L=22$	$L=24$	$L=26$	$L=30$	$L=36$	$L=42$	$L=48$
$C_{\max}/V\ (\times 10^{-3})$	1.031(16)	0.930(5)	0.866(15)	0.777(8)	0.735(7)	0.708(9)	0.709(9)
$\delta T_{C,1/2}\ (\times 10^{-2})$	1.158(22)	0.922(5)	0.725(12)	0.475(6)	0.2617(22)	0.1594(16)	0.1031(9)
$\chi_{1,\max}/V\ (\times 10^{-2})$	2.70(4)	2.611(13)	2.61(4)	2.604(25)	2.758(23)	2.91(3)	3.077(26)
$\delta T_{\chi_1,1/2}\ (\times 10^{-2})$	1.067(16)	0.858(4)	0.681(10)	0.452(4)	0.2531(19)	0.1544(15)	0.1011(8)
$\chi_{2,\max}/V\ (\times 10^{-3})$	2.33(4)	2.026(10)	1.79(4)	1.500(18)	1.299(16)	1.151(18)	1.106(19)
$\delta T_{\chi_2,1/2}\ (\times 10^{-2})$	2.3(4)	1.49(6)	1.09(10)	0.625(16)	0.307(5)	0.1774(26)	0.1111(14)
$V_{L,\min}$	0.6384(4)	0.64085(13)	0.6423(4)	0.64447(23)	0.64530(20)	0.64582(26)	0.64567(23)
$\delta T_{V_L,1/2}\ (\times 10^{-2})$	1.1064(17)	0.887(5)	0.702(11)	0.464(4)	0.2580(21)	0.1579(15)	0.1024(9)

Fig. 7 we may extract the volume dependence of $C_{\max}$ (see Fig. 8). Our estimates for the critical exponents are given in the last part of Table III.

We have also estimated the reduced cumulant V_L proposed by Challa *et al.*[19]:

$$V_L = 1 - \frac{\langle E^4 \rangle}{3\langle E^2 \rangle^2} \tag{23}$$

This variable is expected to approach 2/3 if the probability distribution of energy is described by a single Gaussian form, as for the case of a second-

Table III

Peak height[a]

	σ	a	c
$C_{\max}$	1.04(5)	0.0004(3)	4(2)
$\chi_{1,\max}$	1.15(4)	0.005(2)	40(40)
$\chi_{2,\max}$	0.95(9)	0.002(2)	12(5)
$C_{\max}$	1	0.000679(9)	2.6(4)
$\chi_{1,\max}$	1	0.03150(29)	−157 (12)
$\chi_{2,\max}$	1	0.000973(20)	14.4(9)

Peak Width[b]

	σ	a	c
$\delta T^{-1}_{C,1/2}$	1.07(4)	0.0037(18)	−3(17)
$\delta T^{-1}_{\chi_1,1/2}$	1.06(4)	0.0043(18)	0(15)
$\delta T^{-1}_{\chi_2,1/2}$	1.09(6)	0.003(2)	−40(20)
$\delta T^{-1}_{C,1/2}$	1	0.00899(9)	−34(4)
$\delta T^{-1}_{\chi_1,1/2}$	1	0.00911(8)	−26(3)
$\delta T^{-1}_{\chi_2,1/2}$	1	0.00876(12)	−79(6)

Ising model[c]

O	σ	a
$C_{\max}$	0.10(1)	0.34 (2)
$\chi_{\max}$	0.67(1)	0.25 (1)
$\delta T^{-1}_{\chi,1/2}$	0.52(1)	0.069(3)
$2/3 - V_L$	−0.85(1)	14 (1)

[a] Results of the three parameter fit of the form $aV^{\sigma} + c$ for the peak height using the data for $L = 30$–48. Also shown are the two-parameter fits with $\sigma = 1$.

[b] Same as in the first part of the table, for the inverse of the peak width $\delta T^{-1} = aV^{\sigma} + c$.

[c] Results of the two-parameter fit of the form $O = aV^{\sigma}$ for the Ising model using the data for $L = 16$–48.

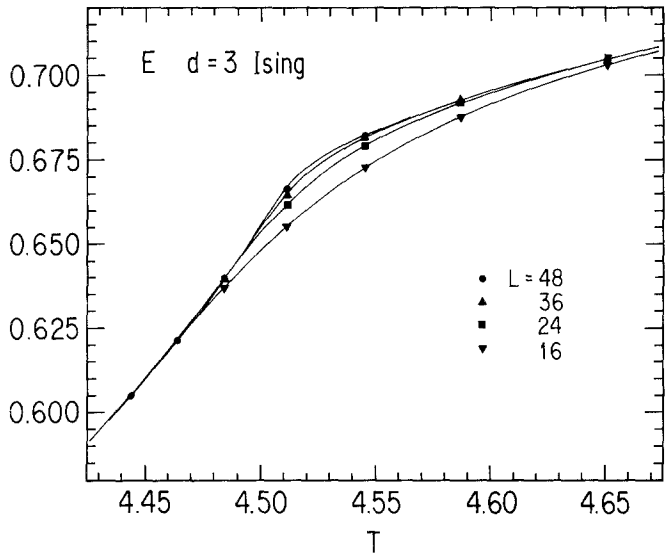

Fig. 6. Internal energy E for the Ising model as a function of T for various lattice sizes. The solid lines are an interpolation of the data points by the spectral density method.

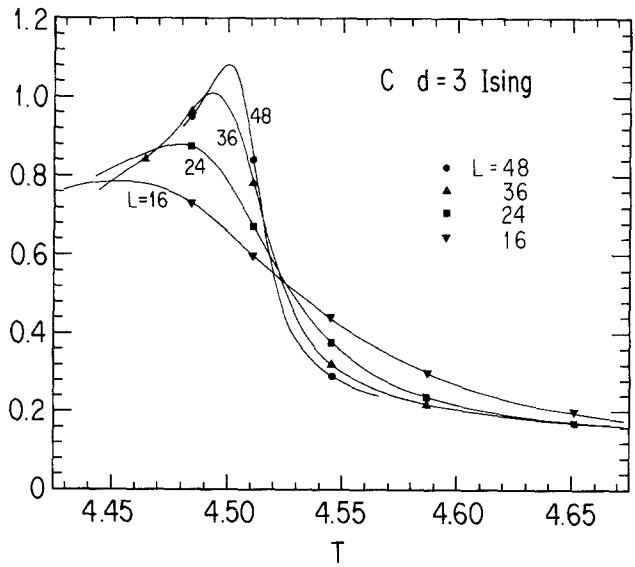

Fig. 7. Specific heat for the Ising model as a function of T for various lattice sizes. The meaning of the lines is the same as in Fig. 6.

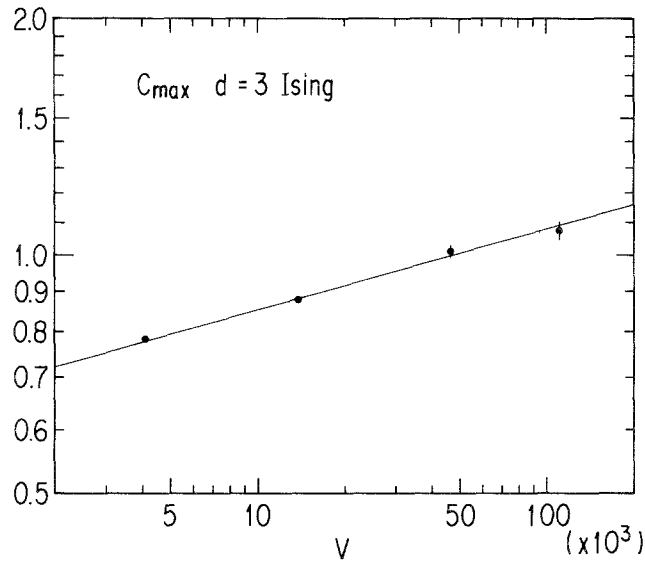

Fig. 8. Peak height of the specific heat C for the Ising model as a function of the volume. The solid line represents the two-parameter fit given in the last part of Table III.

order transition, or otherwise it deviates from this value. Therefore, this variable is expected to give an interesting indicator for the order of a phase transition. In Figs. 9a and 9b we plot V_L as a function of T for the Potts and Ising models. Figure 10 shows the peak values of $2/3 - V_L$ as functions of V (see Table II for numerical values). One clearly observes that $V_{L,\min}$ for the Potts model approaches a finite value, whereas it vanishes for the Ising case as $V \to \infty$. We estimate that

$$\lim_{L \to \infty} V_{L,\min} = 0.6460(2) \tag{24}$$

for the Potts model, and

$$2/3 - V_{L,\min} \propto V^{-\zeta}, \qquad \zeta = 0.85(1) \tag{25}$$

for the Ising model.

4.3. Susceptibility

The order parameters $\langle \Phi_1 \rangle$ and $\langle \Phi_2 \rangle$ and the corresponding susceptibilities χ_1 and χ_2 divided by V are presented in Figs. 11 and 12 as functions of T for various lattice sizes. We see that the behavior of the order

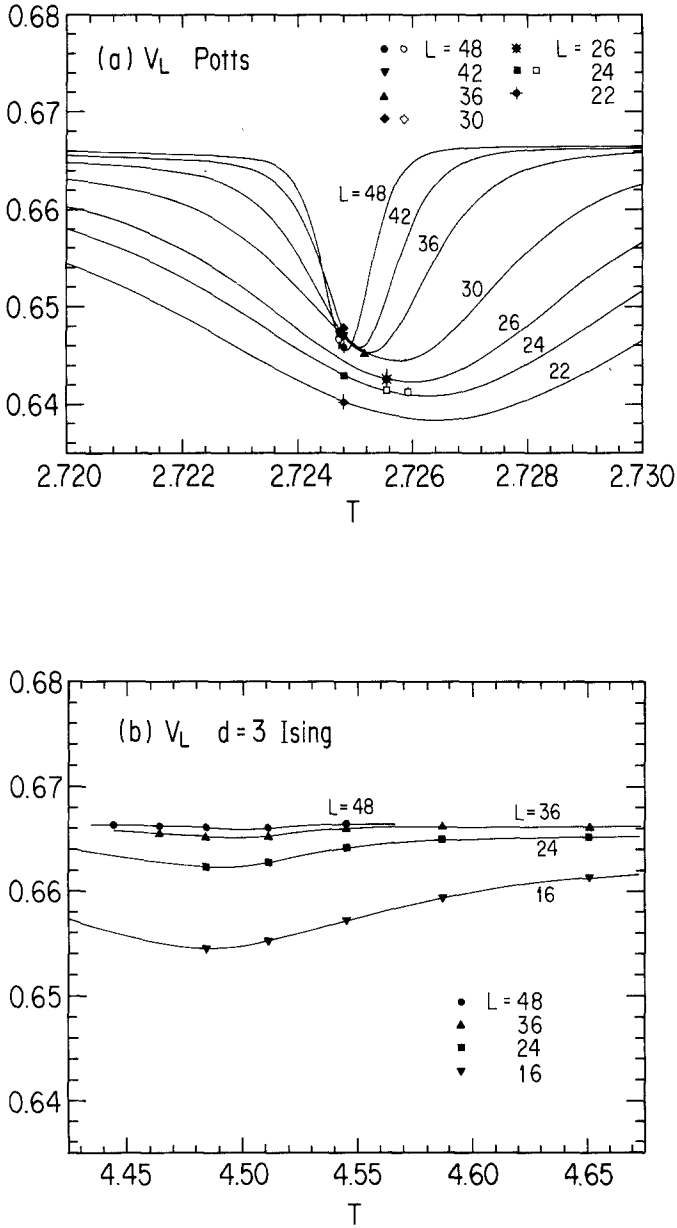

Fig. 9. (a) Reduced cumulant V_L as a function of T for various lattice sizes. The meaning of the lines and symbols is the same as in Fig. 3. (b) Same as (a), for the Ising model. The meaning of the lines is the same as in Fig. 6.

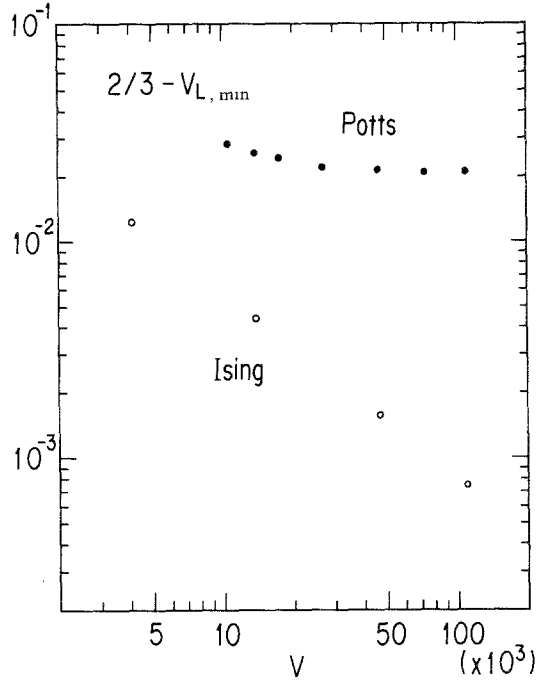

Fig. 10. Peak values of $2/3 - V_L$ as a function of the volume for both the Potts and Ising models.

parameters is similar to that of E, and the susceptibilities similar to C; the curves of $\langle \Phi_i \rangle$ for different sizes cross each other at an almost fixed point, and those of χ_i exhibit progressively more conspicuous peaks as V increases. The numerical values of the peak heights $\chi_{i,\max}$ and the width $\delta T_{\chi_i,1/2}$ are listed in Table II. We apply again a three- as well as two-parameter fits to these quantities. The results are depicted in Fig. 13 and are also tabulated in the first two parts of Table III. The inverse of the peak width $\delta T^{-1}_{\chi_i,1/2}$ increases linearly with the volume. We note, however, that the curve for the peak height for χ_1 slightly deviates from a linear behavior. This may be attributed to the rather artificial definition of Φ_1, for which we separated the complex plane into three parts. For the more naturally defined Φ_2, the peak height beautifully scales linearly. This behavior is again contrasted with a second-order case of the Ising model; see Fig. 14 for the shape of $\langle \Phi \rangle \equiv \langle |(1/V)\sum_i s_i| \rangle$ and $\chi \equiv V(\langle \Phi^2 \rangle - \langle \Phi \rangle^2)$, and Fig. 15 for the height and width for several volumes. Estimates of the critical exponents are listed in the last part of Table III.

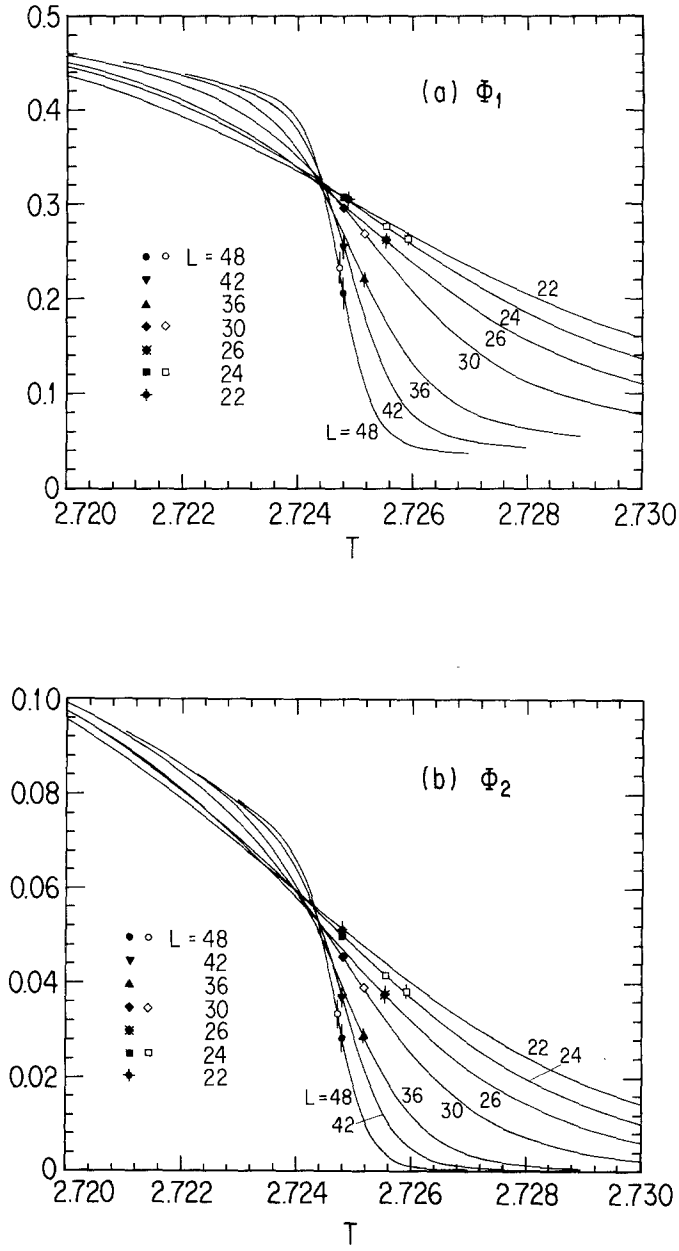

Fig. 11. Order parameter (a) $\langle \Phi_1 \rangle$ and (b) $\langle \Phi_2 \rangle$ as a function of T for various lattice sizes. The meaning of the lines and symbols is the same as in Fig. 3.

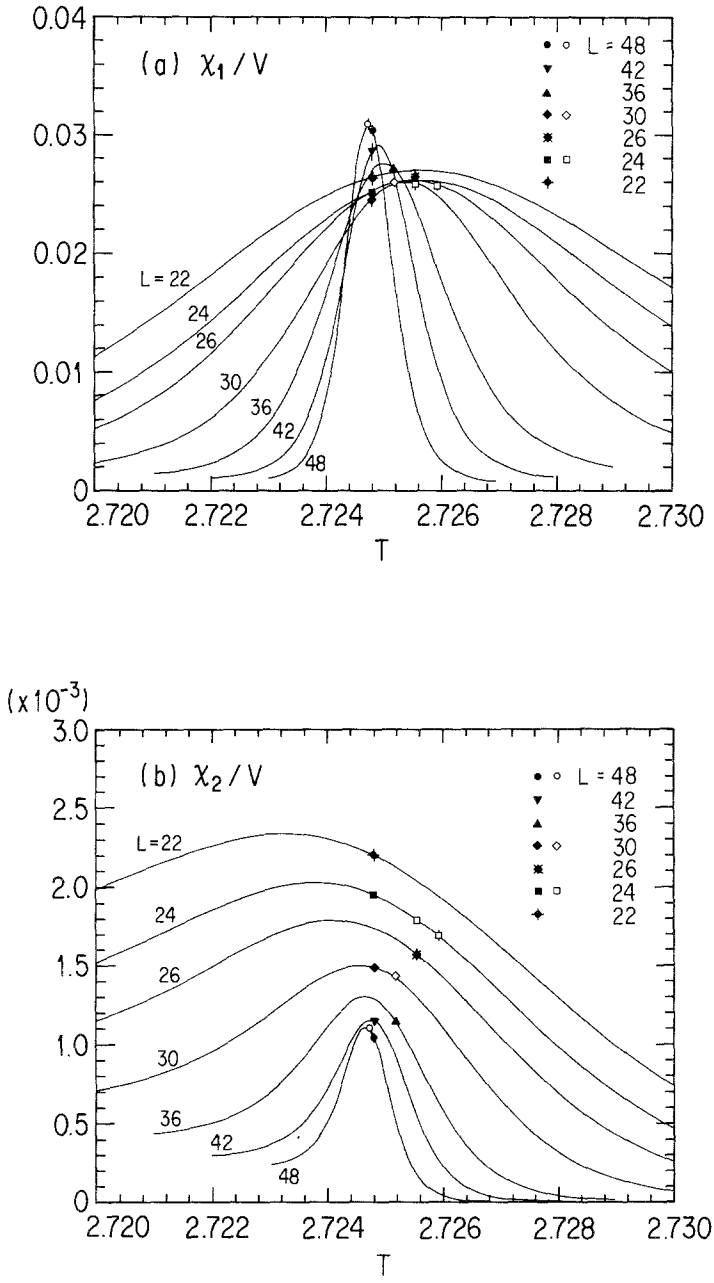

Fig. 12. Susceptibility (a) χ_1 and (b) χ_2 normalized by the volume as a function of T for various lattice sizes. The meaning of the lines and symbols is the same as in Fig. 3.

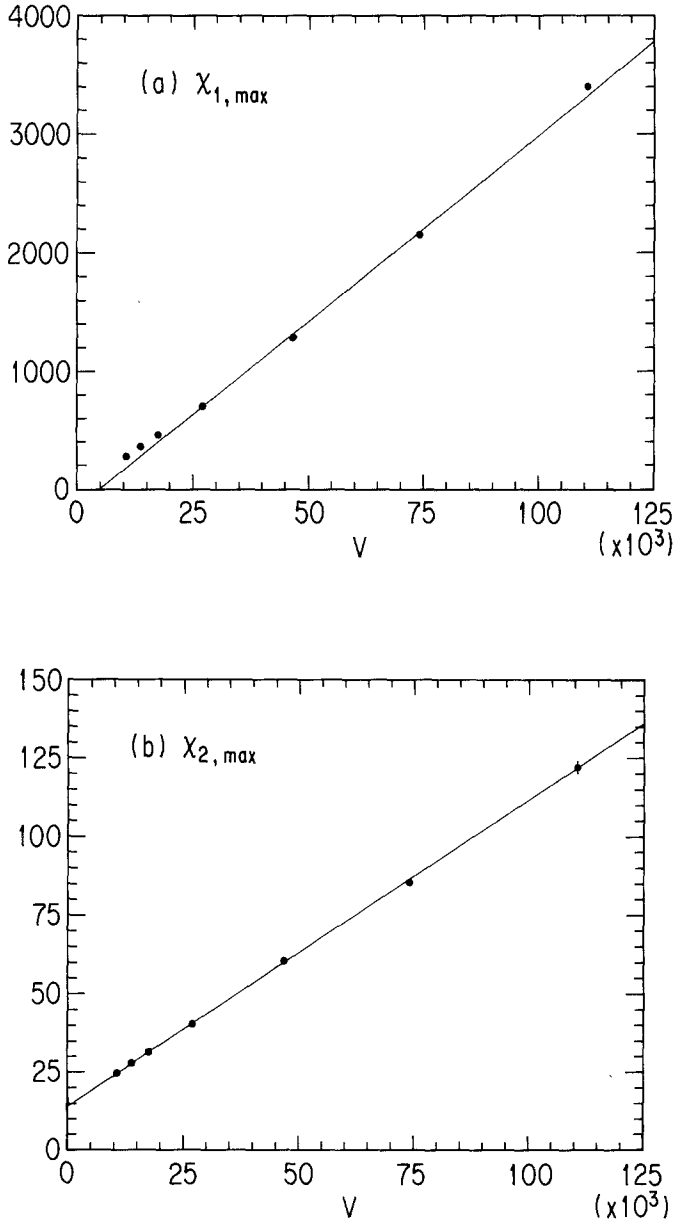

Fig. 13. Peak height of (a) χ_1 and (b) χ_2 and the inverse of the peak width of (c) χ_1 and (d) χ_2 as a function of the volume. The solid line represents the two-parameter fit given in the first two parts of Table III.

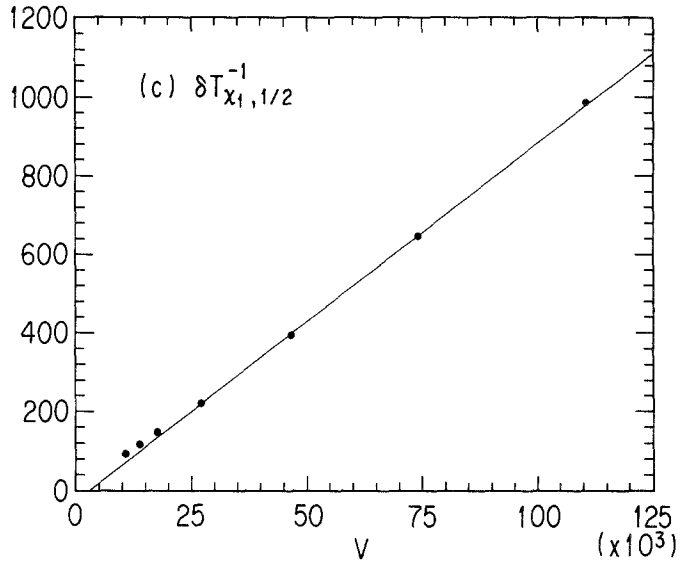

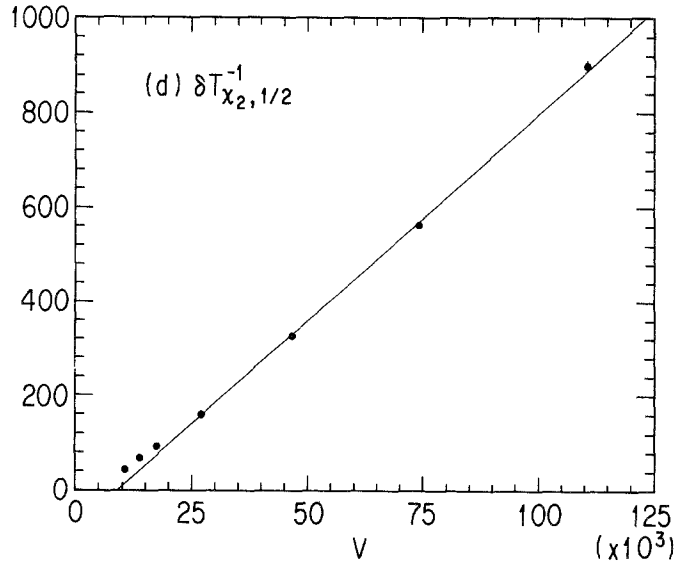

Fig. 13. (*Continued*)

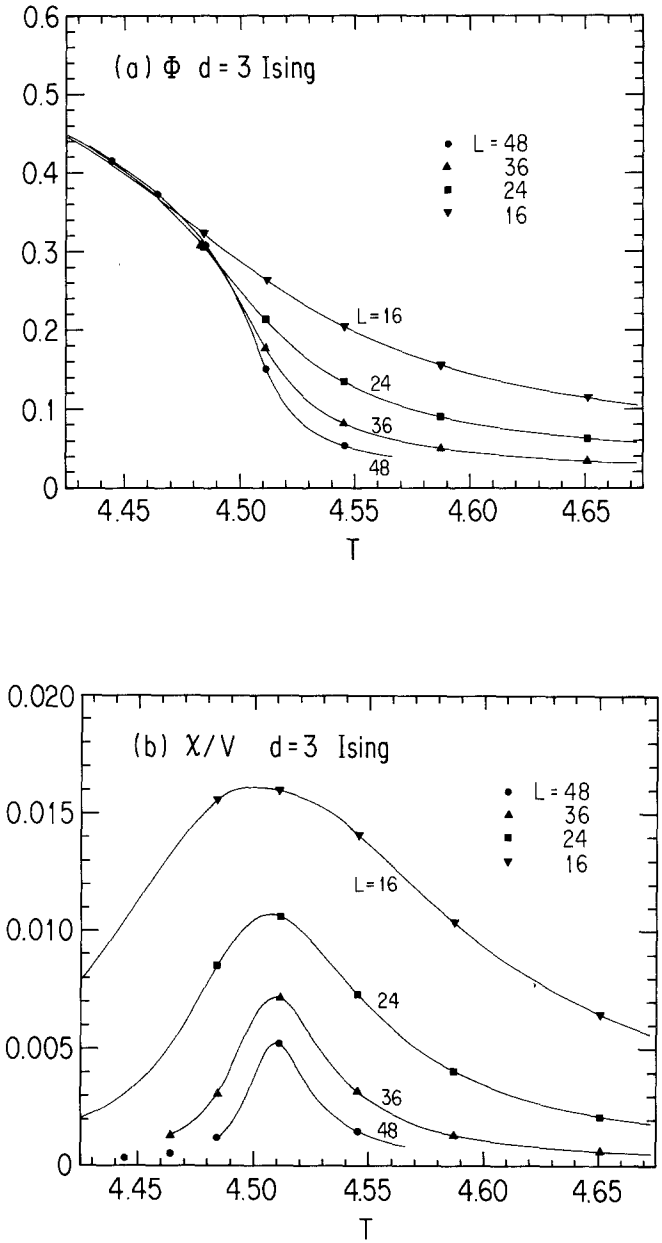

Fig. 14. (a) Order parameter $\langle \Phi \rangle$ and (b) the susceptibility χ normalized by the volume for the Ising model as a function of T for various lattice sizes. The meaning of lines is the same as in Fig. 6.

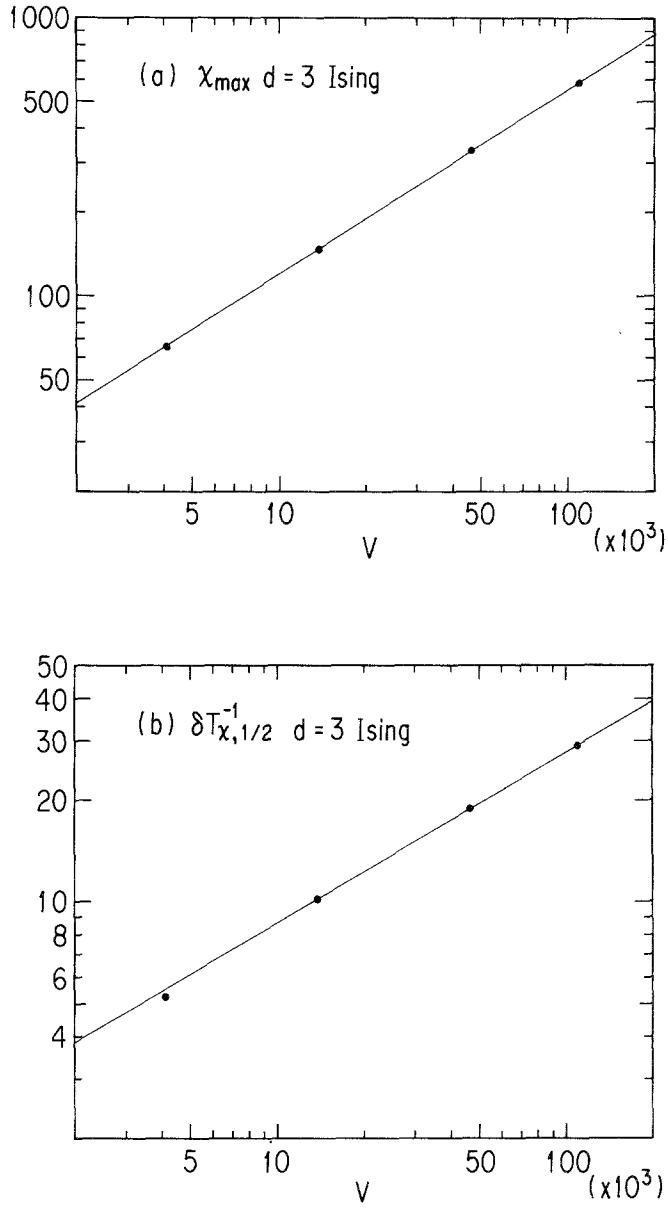

Fig. 15. (a) Peak height and (b) the inverse of the peak width of χ for the Ising model as a function of the volume. The solid line represents the two-parameter fit given in the last part of Table III.

Table IV. Critical Temperature Defined As the Position of the Peak of the Specific Heat, Susceptibilities, and V_L for Various Lattice Sizes

L	C	χ_1	χ_2	V_L
22	2.72461(21)	2.72565(23)	2.72327(19)	2.72638(22)
24	2.72487(6)	2.72568(6)	2.72379(5)	2.72622(6)
26	2.72491(17)	2.72551(18)	2.72411(15)	2.72595(17)
30	2.72505(7)	2.72539(8)	2.72456(6)	2.72570(7)
36	2.72486(6)	2.72501(6)	2.72465(5)	2.72522(6)
42	2.72485(6)	2.72491(6)	2.72475(6)	2.72507(6)
48	2.72471(6)	2.72474(5)	2.72465(5)	2.72485(5)

4.4. The Critical Temperature of the Potts Model

Definition of the critical temperature is ambiguous on a finite lattice. We define it here expediently as the position of the peak of the specific heat, the susceptibilities, and V_L. The critical temperature $T_c(V)$ estimated with this definition is given in Table IV, and is displayed in Fig. 16 as a

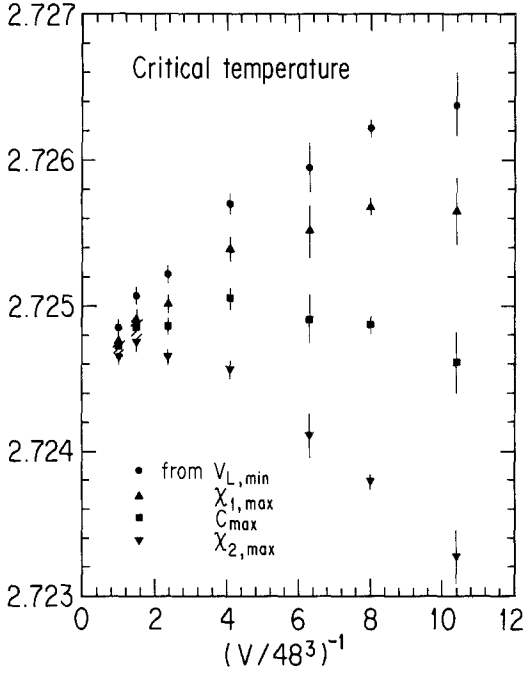

Fig. 16. Critical temperature defined as the peak position of the specific heat, susceptibilities, and V_L as a function of the inverse volume.

function of the inverse volume. We observe that $T_c(V)$, which scatters over a considerably wide range of values for a smaller volume, converges remarkably well to a single value as $V \to \infty$. Allowing for the downward trend seen for the two largest lattice sizes, we estimate the critical temperature at the infinite volume to be

$$T_c(\infty) = 2.7246(2) \qquad [\beta_c(\infty) = 1/T_c(\infty) = 0.36703(3)] \tag{26}$$

It is worth noting that the size dependence of $T_c(V)$ is not quite linear in V^{-1} as presumed in a simple model of a first-order phase transition,[5] but actually shows a more complex behavior [see, e.g., $T_c(V)$ from $C_{\max}$ and $\chi_{2,\max}$]. It is obvious that, if one estimates $T_c(\infty)$ by a linear extrapolation from the data for $L \leqslant 30$, one would obtain an incorrect estimate of $T_c(\infty)$.

4.5. Summary

From the first two parts of Table III we extract the "critical exponent" for the $q = 3$ Potts model to be[6]

$$\begin{aligned} &\alpha/\nu = 3.12(15), \qquad \nu = 0.312(12) \qquad [1/\nu = 3.21(12)] \\ &\gamma/\nu = 2.9(3) \end{aligned} \tag{27}$$

For the three-dimensional Ising model we obtain

$$\alpha/\nu = 0.30(3), \qquad \nu = 0.64(1), \qquad \gamma/\nu = 2.01(3) \tag{28}$$

These indices are compared with the estimates of earlier work[7]:

$$\begin{aligned} &\alpha/\nu = 0.175,^{(26)}\ 0.16(3)^{(29)} \\ &\nu = 0.629(4),^{(27)}\ 0.6295(10),^{(28)}\ 0.634(10),^{(29)}\ 0.6303(14)^{(30)} \\ &\gamma/\nu = 1.98(2),^{(26)}\ 1.964(3)^{(31)} \end{aligned} \tag{29}$$

The values of (27) show that the $q = 3$ Potts model obeys finite-size scaling precisely as expected for a genuine first-order phase transition.

5. CORRELATION LENGTH

In this section we study the finite-size behavior of the correlation length ξ. We present our result in terms of a mass gap defined by the

[5] This prediction is based on a double Gaussian model,[19] and it may be disturbed if there is a small background part.

[6] This may be compared with $\alpha = 0.52 \pm 0.16$, $\gamma = 0.72 \pm 0.22$, and $\nu = 0.51 \pm 0.04$ by Herrmann.[7]

[7] Our value of α/ν for $L \geqslant 16$ is larger than the known value. The precise measurement of α/ν, however, require large lattices, since the growth of $C_{\max}$ is rather slow. In fact, if we use only the data of $L = 36$ and 48, we obtain $\alpha/\nu = 0.2(1)$.

inverse of the correlation length, since ξ itself varies over too wide a range in the vicinity of the transition point.

5.1. Naive Definition

We first consider the mass gap defined in terms of the unsubtracted correlation function $C(z)$ in (10). On an infinite lattice, it is given by

$$m(T) = \frac{1}{\xi(T)} = -\lim_{z \to \infty} \frac{1}{z} \log C(z) \tag{30}$$

In the symmetric phase above the transition point $T > T_c$, there is a unique ground state. The first excited state has a finite energy separation from it, and the mass gap defined by (30) represents this energy difference. In the broken phase $T < T_c$, on the other hand, the ground state is threefold degenerate, each of which has a nonvanishing expectation value of $\langle \Phi_i \rangle$. The mass gap $m_{V=\infty}$ vanishes in this case. The difference between a first- and a second-order transition is seen in the behavior of $m_{V=\infty}(T)$ as T decreases toward T_c in the symmetric phase. It is expected to remain finite for a first-order case, whereas it vanishes as $m_{V=\infty}(T) \sim (T - T_c)^{\nu}$ for second-order transitions.

Let us recapitulate how these infinite-volume behaviors are modified on a finite lattice size. For a first-order transition[18,32] the symmetric and the broken ground-state levels at infinite volume cross each other at $T = T_c$. On a finite volume, the tunneling close to T_c mixes these levels and results in a small but finite energy gap between the lowest and the next-lowest levels at $T \sim T_c$. The large-distance behavior of the unsubtracted correlation function $C(z)$ close to T_c is dominated by this gap and therefore the mass gap $m_V(T)$ extracted from it by the modification of (30) appropriate for a finite volume varies continuously across T_c. Away from T_c, the tunneling becomes increasingly rare and $m_V(T)$ for sufficiently large V will approach the infinite-volume values. With an increasing volume V the tunneling occurs only in a narrower range of T around T_c. We therefore expect that a family of functions $m = m_V(T)$ shows an increasingly sharper rise around the transition point as V increases, eventually becoming discontinuous at $V = \infty$. This means that the curves of $m_V(T)$ for different V cross each other at a volume-dependent value $T_{c\gamma}(V)$; $m_V(T)$ should increase with V for $T > T_{c\gamma}(V)$, while it decreases for $T < T_{c\gamma}(V)$.

This interesting behavior is contrasted with the second-order case for which the infinite-volume mass gap vanishes as $m_{V=\infty}(T) \sim (T - T_c)^{\nu}$ for $T \geqslant T_c$ and stays zero for $T \leqslant T_c$. There we expect for $V \to \infty$ a smooth

approach to this function from above. The curves of $m_V(T)$ for different V will not cross.

We applied the spectral density method to calculate the zero-momentum projected correlation function for continuous values of β. We then fit $C(z)$ with the hyperbolic cosine form

$$C(z) = A \cosh m\left(z - \frac{L}{2}\right) \tag{31}$$

with the fitting range $z_{\min} \leqslant z \leqslant L/2$. We used $z_{\min} = 4$, since stable results were obtained for $z_{\min} \geqslant 4$. Figure 17 shows a typical example of $C(z)$ with the solid line representing the hyperbolic cosine fit. To demonstrate the effectiveness of the spectral density method, we compare the result of this method for the mass gap $m_V(T)$ calculated with the data at $\beta_0 = 0.3670$ on a 48^3 lattice to the value of ref. 10 evaluated by the direct simulation at each T. The result is shown in Fig. 18. We recognize a good agreement between the two. The curves in Fig. 19 show the volume dependence of $m_V(T)$. Apparent in this figure are an increasingly rapid rise of $m_V(T)$ with increasing V and a crossing of the curves. This behavior is in distinct contrast with the mass gap for the three-dimensional Ising model, which we

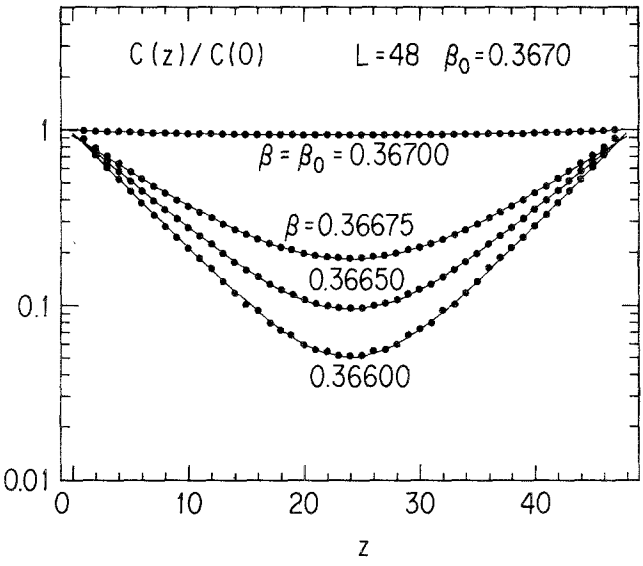

Fig. 17. Examples of the unsubtracted correlation function $C(z)$ on a 48^3 lattice obtained by the spectral density method using the data at $\beta_0 = 0.3670$ as input. The solid lines represent a hyperbolic cosine fit (31) with $z_{\min} = 4$.

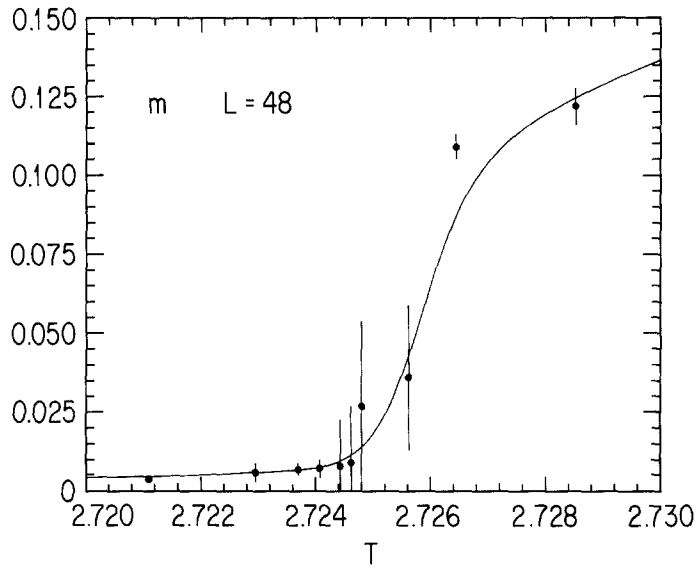

Fig. 18. Mass gap extracted from the unsubtracted correlation function on a 48^3 lattice. The solid line is obtained with the help of the spectral density method using the data at $\beta_0 = 0.3670$. The values of the data points are taken from ref. 10.

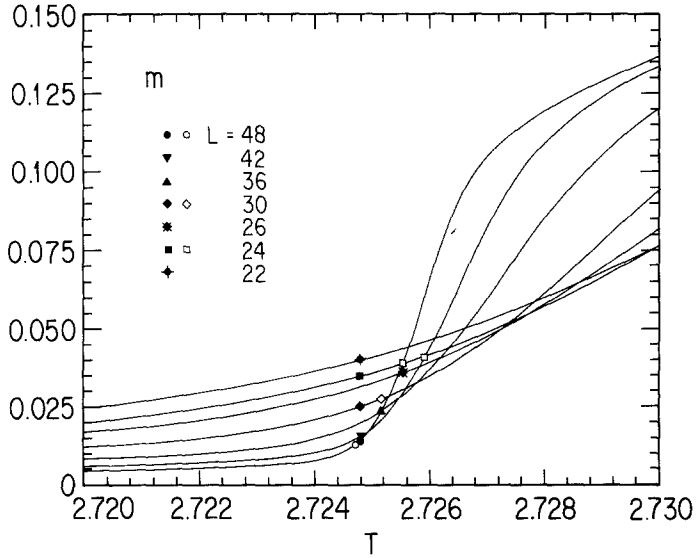

Fig. 19. Mass gap extracted from the unsubtracted correlation function as a function of T for various lattice sizes. The meaning of the lines and symbols is the same as in Fig. 3.

depict in Fig. 20; the curves of $m_V(T)$ approach the asymptotic value smoothly from above. This exemplifies clearly the difference between a first- and a second-order phase transitions.

Let us comment on the "critical exponent" for a first-order transition.[7,16] As is clear from the above argument, the correlation length ξ becomes very large and it may eventually exceed the lattice size even for $T > T_c$ close to the critical point (see Fig. 19). One cannot parametrize, however, this behavior in terms of the critical exponent of the form $\sim |T - T_c|^{-\nu}$, due to the rapid change of the shape of $\xi_V(T)$ as V varies; if one were to extract ν from the finite-size behavior, it would vary with the size of the lattice.

5.2. Physical Mass Gap

By the physical mass gap m_{phys} we mean the energy difference between the ground and the first excited states in each phase. Extraction of this quantity is quite complicated on a finite lattice due to the mixing of levels through tunneling. It is, in principle, possible to extract m_{phys} of each phase by adding subdominant terms in (31). Attempts were made in refs. 17 and 33 for the Ising model in two and four dimensions and in ref. 10 for the

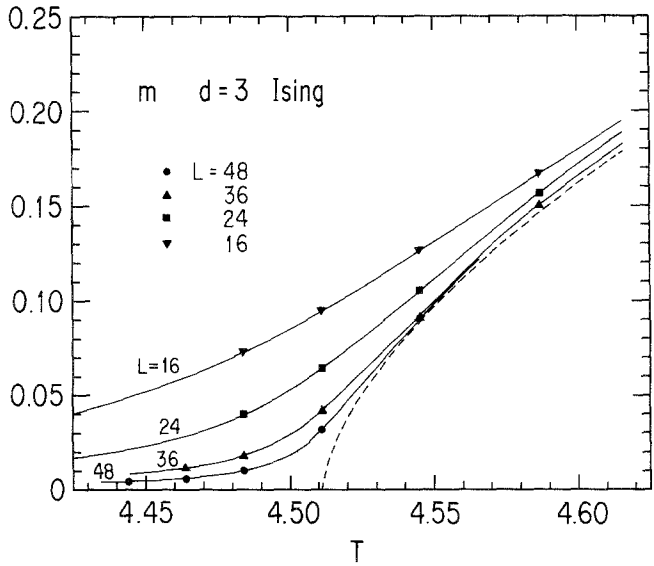

Fig. 20. Mass gap for the Ising model as a function of T for various lattice sizes. The solid lines are an interpolation of the data points by the spectral density method. The dashed line showing $m_{V=\infty}(T) = 0.748 \times (T - T_c)^{\nu}$ is an estimate of the infinite-volume limit obtained by using the known values of $T_c = 4.51154$ and $\nu = 0.629$.[27]

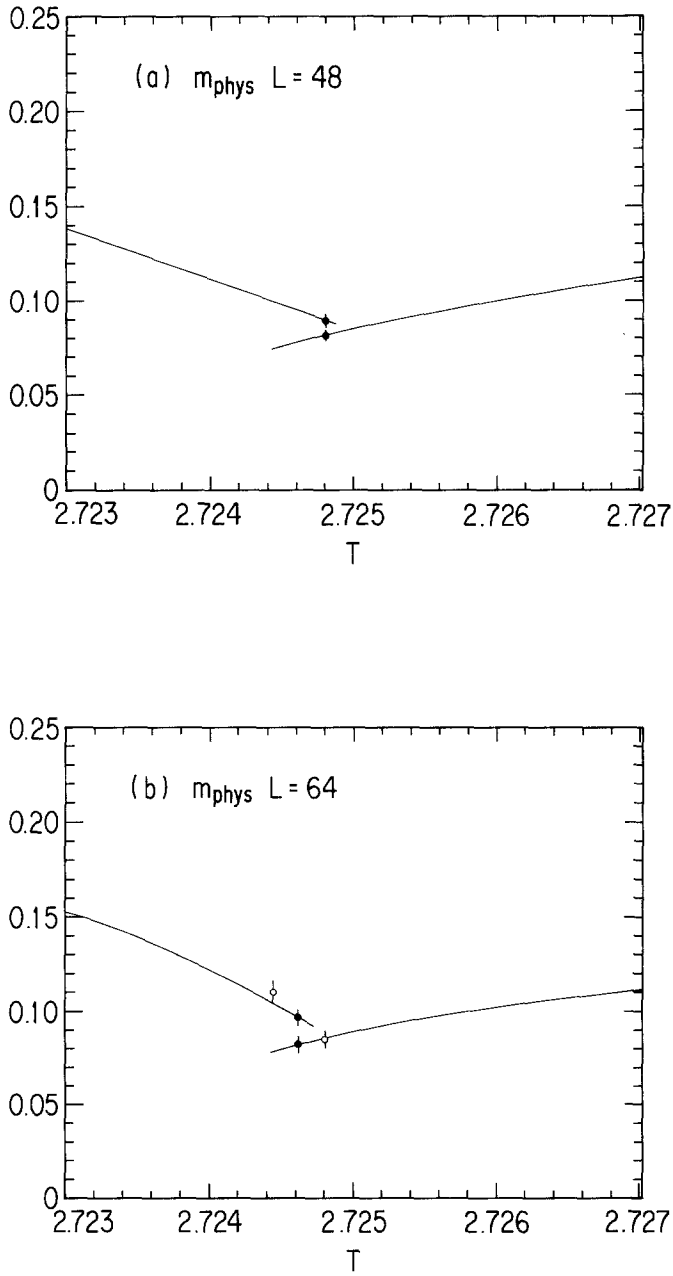

Fig. 21. Physical mass gap as a function of T for a lattice size of (a) 48^3 and (b) 64^3. The meaning of the lines and symbols is the same as in Fig. 3.

Potts model. For a first-order phase transition, however, this is quite complicated, since one has to extract the physical mass gap, expected to be discontinuous at the transition point, from among a multiple of levels competing against each other.

In this paper we take the practical resort of dividing the run showing the flipflop behavior into two phases and evaluate m_{phys} separately for the two states. The separation of a run is done by picking the sweep interval by an inspection of the time history of the order parameter. For $L = 64$, we can use four runs with 1×10^6 sweeps, since they do not exhibit a flipflop. For $L = 48$, we discarded a few thousand sweeps on both sides of the interval where the system flipped from one phase to the other. It is difficult, however, to apply this method to smaller lattices due to a short flipflop interval and large fluctuations.

To extract m_{phys} for the symmetry-broken (ordered) phase, we used the form

$$C(z) = \langle \Phi_1 \rangle^2 + A \cosh m_{\text{phys}} \left(z - \frac{L}{2} \right) \tag{32}$$

while for the symmetric phase we assumed a function of the form (31).

In Fig. 21 we give the physical mass gap m_{phys} as a function of T in the vicinity of the transition point. We observe that the value of the physical mass gap does not depend on the lattice size. m_{phys} stays at a finite value and is discontinuous at $T = T_c$. The magnitude of m_{phys} is about 0.1, in agreement with the value reported in refs. 10 and 11.

6. CONCLUSION

In this paper we have studied the finite-size behavior of the thermodynamic quantities and the correlation length of the three-state Potts model in three dimensions, with a comparative study of the three-dimensional Ising model in addition. We found that the Potts model exhibits the finite-size behavior most typical of a first-order phase transition, and we did not detect any sign of criticality, though the physical correlation length becomes somewhat large at the transition point. Specifically we observed:

(i) Quantities characterizing fluctuations, i.e., specific heat and magnetic susceptibilities, show a finite-size scaling which depends only linearly on the volume.

(ii) The correlation length extracted from the unsubtracted correlation function shows a finite-size behavior characteristic of a first-order transition, i.e., the step-function-type singularity is developed as $V \to \infty$.

(iii) The physical correlation length stays at a finite value and is discontinuous at the transition point.

The present analysis has shown that the finite-size scaling test is a very powerful tool to determine the order of a phase transition even for a rather subtle case without subjective elements coming into the judgment.

ACKNOWLEDGMENTS

Numerical computation for this work was made on the HITAC S820/80 at KEK. M.F. and A.U. thank the Theory Division of KEK for its warm hospitality while this work was being carried out. This work was supported in part by grant-in-aids of the Ministry of Education (01460017, 01740165, and 01790220).

REFERENCES

1. R. B. Potts, *Proc. Camb. Phil. Soc.* **48**:106 (1952); T. Kihara, Y. Midzuno, and J. Shizume, *J. Phys. Soc. Japan* **9**:681 (1954).
2. F. Y. Wu, *Rev. Mod. Phys.* **54**:235 (1982).
3. L. D. Landau, *Phys. Z. Sowjetunion* **11**:26 (1937).
4. R. J. Baxter, *J. Phys. C* **6**:L445 (1973).
5. H. W. J. Blöte and R. H. Swendsen, *Phys. Rev. Lett.* **43**:799 (1979).
6. S. J. Knak Jensen and O. G. Mouritsen, *Phys. Rev. Lett.* **43**:1736 (1979).
7. H. J. Herrmann, *Z. Phys. B* **35**:171 (1979).
8. W. G. Wilson and C. A. Vause, *Phys. Rev. B* **36**:587 (1987); M. S. S. Challa and J. H. Hetherington, *Phys. Rev. A* **38**:6324 (1988).
9. J. P. Straley and M. E. Fisher, *J. Phys. A* **6**:1310 (1973); S. Miyashita, D. D. Betts, and C. J. Elliott, *J. Phys. A* **12**:1605 (1979), and references therein.
10. R. V. Gavai, F. Karsch, and B. Petersson, *Nucl. Phys. B* **322**:738 (1989).
11. M. Fukugita and M. Okawa, *Phys. Rev. Lett.* **63**:13 (1989).
12. M. E. Fisher, in *Critical Phenomena*, M. S. Green, ed. (Academic Press, New York, 1971).
13. M. N. Barber, in *Phase Transitions and Critical Phenomena*, Vol. 8, C. Domb and J. L. Lebowitz, eds. (Academic Press, New York, 1983).
14. B. Nienhuis and M. Nauenberg, *Phys. Rev. Lett.* **35**:477 (1975).
15. Y. Imry, *Phys. Rev. B* **21**:2042 (1980).
16. M. E. Fisher and A. N. Berker, *Phys. Rev. B* **26**:2507 (1982).
17. H. W. J. Blöte and M. P. Nightingale, *Physica* **112A**:405 (1982).
18. V. Privman and M. E. Fisher, *J. Stat. Phys.* **33**:385 (1983).
19. M. S. S. Challa, D. P. Landau, and K. Binder, *Phys. Rev. B* **34**:1841 (1986).
20. I. R. McDonald and K. Singer, *Disc. Faraday Soc.* **43**:40 (1967); see also M. Falcioni *et al.*, *Phys. Lett.* **108B**:331 (1982).
21. A. M. Ferrenberg and R. Swendsen, *Phys. Rev. Lett.* **61**:2635 (1988); see also *Phys. Rev. Lett.* **63**:1195 (1989).
22. T. G. Lewis and W. H. Payne, *J. ACM* **20**:456 (1973).
23. B. Efron, *SIAM Rev.* **21**:460 (1979).
24. A. Gonzalez-Arroyo, M. Okawa, and Y. Shimizu, *Phys. Rev. Lett.* **60**:487 (1988).

25. A. Hasenfratz and P. Hasenfratz, *Nucl. Phys. B* **235**:1 (1988).
26. M. N. Barber, R. B. Pearson, D. Toussaint, and J. L. Richardson, *Phys. Rev. B* **32**:1720 (1985).
27. G. S. Pawley, R. H. Swendsen, D. J. Wallace, and K. G. Wilson, *Phys. Rev. B* **29**:4030 (1984).
28. G. Bhanot *et al.*, *Phys. Rev. Lett.* **59**:803 (1987).
29. P.-Y. Lai and K. K. Mon, *Phys. Rev. Lett.* **62**:2608 (1989).
30. N. A. Alves, B. A. Berg, and R. Villanova, FSU-SCRI-89-75 (1989).
31. G. Bhanot, D. Duke, and R. Salvador, *Phys. Rev. B* **33**:7841 (1986).
32. F. Iglói and J. Sólyom, *J. Phys. C* **16**:2833 (1983); C. J. Hamer, *J. Phys. A* **16**:3085 (1983).
33. K. Jansen *et al.*, *Phys. Lett.* **213B**:203 (1988).